Observation of a metal-to-insulator transition with both Mott-Hubbard and Slater characteristics in Sr_{2}IrO_{4} from time-resolved photocarrier dynamics

D. Hsieh, F. Mahmood, D. H. Torchinsky, G. Cao, and N. Gedik

Phys. Rev. B **86**, 035128 — Published 18 July 2012

DOI: 10.1103/PhysRevB.86.035128

Observation of a metal-to-insulator transition with both Mott-Hubbard and Slater characteristics in Sr_2IrO_4 from time-resolved photo-carrier dynamics

D. Hsieh,[1] F. Mahmood,[1] D. H. Torchinsky,[1] G. Cao,[2,3] and N. Gedik[1]

[1] *Department of Physics, Massachusetts Institute of Technology, Cambridge, MA 02139, USA*
[2] *Center for Advanced Materials, University of Kentucky, Lexington, Kentucky 40506, USA*
[3] *Department of Physics and Astronomy, University of Kentucky, Lexington, Kentucky 40506, USA*

(Dated: June 12, 2012)

We perform a time-resolved optical study of Sr_2IrO_4 to understand the influence of magnetic ordering on the low energy electronic structure of a strongly spin-orbit coupled J_{eff}=1/2 Mott insulator. By studying the recovery dynamics of photo-excited carriers, we find that upon cooling through the Néel temperature T_N the system evolves continuously from a metal-like phase with fast (∼50 fs) and excitation density independent relaxation dynamics to a gapped phase characterized by slower (∼500 fs) excitation density dependent bimolecular recombination dynamics, which is a hallmark of a Slater-type metal-to-insulator transition. However our data indicate that the high energy reflectivity associated with optical transitions into the unoccupied J_{eff}=1/2 band undergoes the sharpest upturn at T_N, which is consistent with a Mott-Hubbard type metal-to-insulator transition involving spectral weight transfer into an upper Hubbard band. These findings show Sr_2IrO_4 to be a unique system in which Slater- and Mott-Hubbard type behaviors coexist and naturally explain the absence of anomalies at T_N in transport and thermodynamic measurements.

I. INTRODUCTION

Iridium oxides are unique 5*d* electronic systems in which spin-orbit coupling, electronic bandwidth (W) and on-site Coulomb interactions (U) occur on comparable energy scales. Their interplay can stabilize a novel J_{eff}=1/2 Mott insulating state in which a correlation gap is opened by only moderate Coulomb interactions owing to a spin-orbit coupling induced band narrowing[1]. Depending on the underlying lattice, this insulating state is predicted to realize a variety of exotic quantum phases including antiferromagnetic J_{eff}=1/2 Mott insulators on the perovskite lattice[1–3], correlated topological insulators and semimetals on the pyrochlore lattice[4–6] and topological spin liquids on the hyper-kagome[7] and honeycomb lattices[8]. Even more tantalizing possibilities are predicted to occur upon chemically doping these systems, ranging from high-T_c superconductivity[9,10] to spin-triplet superconductivity[8].

Intensive research has been conducted on the layered perovskite iridate Sr_2IrO_4 owing to its structural and electronic similarities to undoped high-T_c cuprates such as La_2CuO_4[1,9]. The ground state electronic structure of Sr_2IrO_4 consists of a completely filled band with total angular momentum $J_{eff} = 3/2$ and a narrow half-filled $J_{eff} = 1/2$ band near the Fermi level E_F[1,11,12]. The latter is split into an upper Hubbard band (UHB) and lower Hubbard band (LHB) due to on-site Coulomb interactions and exhibits antiferromagnetic ordering of the effective $J_{eff} = 1/2$ moments below a Néel temperature T_N = 240 K[3] analogous to La_2CuO_4. Although this insulating ground state has been established by angle-resolved photoemission spectroscopy[1] and resonant x-ray scattering[11] measurements, whether Sr_2IrO_4 is a Mott-type ($U \gg W$) insulating phase typical of 3*d* transition metal oxides or a Slater-type ($U \approx W$) insulating phase is experimentally unknown and remains a topic of active theoretical debate[10,13,14]. Whereas a Mott-Hubbard type metal-to-insulator transition (MIT) is discontinuous and occurs at temperatures greater or equal to T_N, a Slater-type MIT is continuous and occurs exactly at T_N[15]. Therefore the relevant experimental question is whether heating above T_N brings Sr_2IrO_4 into a paramagnetic insulating phase or into a paramagnetic metallic phase and what the order of the MIT is.

Owing to an absence of clear anomalies at T_N in transport[3,16–18], thermodynamic[17] and optical conductivity data[19], there have been conflicting interpretations about how the insulating gap behaves across T_N. In this article we use time-resolved optical spectroscopy, which is highly sensitive to the existence of energy gaps[20,21], to study the temperature evolution of the electronic structure of Sr_2IrO_4. Taking advantage of qualitatively distinct relaxation dynamics of photo-excited carriers exhibited by gapped and gapless systems, we find a clear change in the ultrafast dynamics across T_N indicating a gap opening concomitant with antiferromagnetic order. Analysis of the long time relaxation dynamics further reveals behavior that is consistent with in-gap spectral weight being continuously transferred to high energies through T_N, supporting a phase transition from low-temperature insulator to high-temperature paramagnetic metal with both Mott-Hubbard and Slater-type characteristics.

II. EXPERIMENTAL DETAILS

In our experiment we used a Ti:Sapphire oscillator producing laser pulses with center wavelength 795 nm ($h\nu$ = 1.56 eV) and near 80 fs duration. The fluence of the pump pulse, which excites electrons across the insulating gap from the occupied J_{eff} = 3/2 and

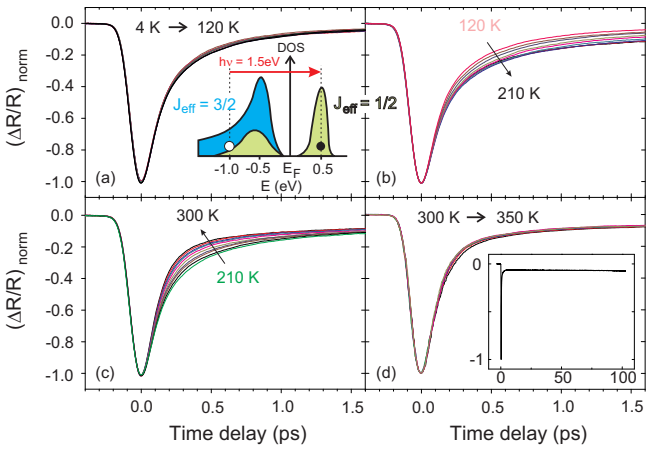

FIG. 1. Normalized time-resolved reflectivity traces $(\Delta R/R)_{norm}$ of Sr_2IrO_4 collected in the temperature ranges (a) 4 K to 120 K, (b) 120 K to 210 K, (c) 210 K to 300 K and (d) 300 K to 350 K. Curves are collected in 10 K intervals with a pump fluence of 15.4 μJ/cm^2. Inset of panel (a) shows a schematic of the low energy electronic density of states (DOS) based on calculations[12]. The red arrow denotes the optical transition being excited by the pump pulse. Inset of panel (d) shows the T = 300 K trace out to 100 ps time delay.

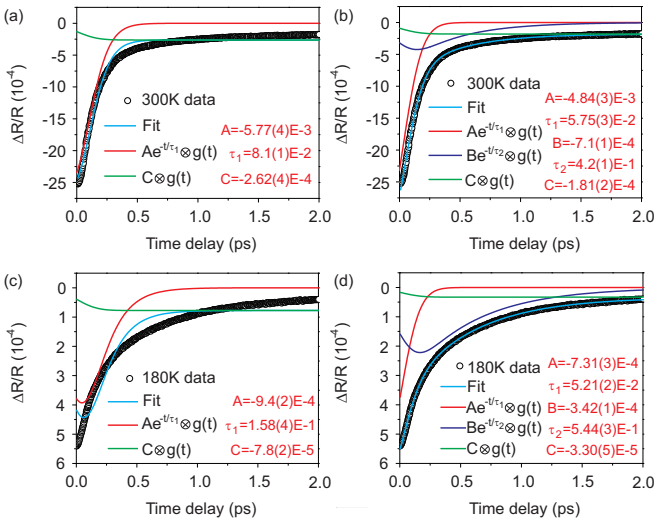

FIG. 2. Transient reflectivity traces taken at T = 300K and F = 15.4μJ/cm^2 and fitted to a (a) single and (b) double exponential decay. Transient reflectivity traces taken at T = 180K and F = 1.9μJ/cm^2 and fitted to a (c) single and (d) double exponential decay. Curves show the overall fit as well as the separate components of the fit. The fitted parameters and their associated fitting errors (in parentheses) are listed in red.

J_{eff} = 1/2 bands to the unoccupied J_{eff} = 1/2 band [inset Fig. 1(a)], was varied with neutral density filters to tune the photo-excited carrier density while the probe fluence was maintained at 4 μJ/cm^2. Both beams were focused to a 70 μm FWHM spot on the (001) cleaved face of the sample. The 80 MHz repetition rate was reduced to 1.6 MHz with a pulse picker to eliminate steady state heating of the sample. Use of a double-modulation scheme[20] provided sensitivity to the fractional change of reflectivity on the order $\Delta R/R \sim 10^{-7}$. Single crystals of Sr_2IrO_4 were grown using a self-flux technique and magnetization measurements show a magnetic ordering temperature at T_N = 240 K[3,17].

III. RESULTS AND ANALYSIS

Figure 1 shows typical time-resolved reflectivity transients measured over a range of temperatures spanning 4 K to 350 K, which have all been normalized to their negative peak values in order to emphasize the recovery dynamics. We note that the temperature here refers to that before the pump excitation, which will be lower than the instantaneous electronic temperatures reached in the ps time windows following photo-excitation. Following the pump excitation, the electronic temperature is elevated above the initial equilibrium temperature and all $\Delta R/R$ traces exhibit a rapid negative spike, which indicates a decrease in reflectivity. Within approximately 1 ps, the reflectivity recovers to a small negative offset that persists beyond 100 ps [inset Fig. 1(d)]. By performing a temperature dependence study we find that the initial ∼1 ps recovery can actually be decomposed into two separate components as follows. Figure 1(a) shows that between 4 K and 120 K there is no discernible change in the recovery dynamics. Upon heating from 120 K to 210 K [Fig. 1(b)], we find no temperature dependence within the first ∼100 fs but observe a clear slowing down of recovery dynamics after this time. Further heating of the sample from 210 K to 300 K again causes no change in the first recovery component but causes the second component to become faster [Fig. 1(c)]. All temperature dependence then completely shuts off above 300 K [Fig. 1(d)]. To understand the physical processes underlying these trends, we perform detailed fits to the $\Delta R/R$ traces.

We fit the un-normalized time-resolved reflectivity transients $[\Delta R/R](t)$ at all temperatures to a convolution $[f \otimes g](t) \equiv \int_{-\infty}^{\infty} f(\xi)g(t-\xi)d\xi$ of a bi-exponential decay function $f(t)$ and a Gaussian instrument resolution function $g(t)$ where:

$$f(t) = \begin{cases} 0 & ;\text{if } t < 0 \\ \mathrm{Ae}^{-t/\tau_1} + \mathrm{Be}^{-t/\tau_2} + \mathrm{C} & ;\text{if } t > 0 \end{cases}$$

and

$$g(t) = \frac{1}{\sigma\sqrt{2\pi}} e^{-\frac{t^2}{2\sigma^2}}$$

where σ is experimentally determined by measuring an autocorrelation of our laser pulses.

To demonstrate that the $[\Delta R/R](t)$ traces are described by a minimum of two exponential decays, we fit $[f \otimes g](t)$ to our data at positive time delays to both a single and double exponential decay. We show fits to the data in two extreme cases: i) data taken at a temperature $T = 300$K and pump fluence $F = 15.4\mu$J/cm^2, where the magnitude of the slower decay component is shown to be smallest [shown later in Fig. 4(c)], ii) data taken at a temperature $T = 180$K and pump fluence $F = 1.9\mu$J/cm^2, where the magnitude of the slower decay component is shown to be largest [shown later in Fig. 4(c)]. Figure 2 shows that in both extremes, the data can only be satisfactorily described by two exponential decays. A decomposition of the fits into its individual components [Fig. 2] shows that the slow component is required to account for the curvature in $\Delta R/R$ around 0.5ps. The fitted parameters listed in red show that their standard error is small, less than the size of the symbols plotted in the all figures. We found that the fit results are not sensitive to changes of order $\pm 40\%$ in their initial estimated values.

A. Fast decay component

We begin by trying to understand the physical origin of the first decay component, which is resolved by our ultrashort laser pulses [Fig. 3(a)]. To investigate whether this fast decay arises from thermalization of photo-excited carriers via carrier-carrier scattering, whose rate should depend on the number of photo-excited carriers[22], we measured τ_1 over a range of pump fluences spanning a photo-excitation density d between $\sim 10^{-5}$ to $\sim 10^{-3}$ photons per iridium site. We estimate d using the expression $d = \frac{N}{n\sigma\xi}$, where N is the number of photons per pump pulse, n is the number of iridium sites per unit volume, σ is the area of the sample illuminated by the pump pulse and ξ is the optical penetration depth of photons with wavelength $\lambda = 795$ nm. The penetration depth ξ is derived through the Beer-Lambert law $\xi = \frac{\lambda}{4\pi k}$[23]. The extinction coefficient k, equal to the imaginary part of the index of refraction, can be calculated using equation (8) in[24] from the amplitude (R) and phase (ϕ) of the reflection coefficient of Sr_2IrO_4. We use available published values of R and ϕ from lightly Rh doped Sr_2IrO_4 thin films[25], whose optical conductivity spectrum is nearly identical to bulk single crystalline Sr_2IrO_4.

A linear behavior of the component amplitude (A) over this fluence range [Fig. 3(b)] shows that the number of photo-excited carriers is indeed proportional to the pump fluence. Figure 3(c) shows that $\tau_1 \approx 50$ fs exhibits no discernible fluence nor temperature dependence between 4 K and 350 K. This implies that the initial decay is not caused by photo-carrier thermalization but more likely by photo-carrier cooling, and that this cooling is not mediated by thermally occupied phonons. The participation of magnons is also negligible because τ_1 is insensitive to T_N. Given that the fast timescale of τ_1 is consistent with typical optical phonon mediated cooling processes and

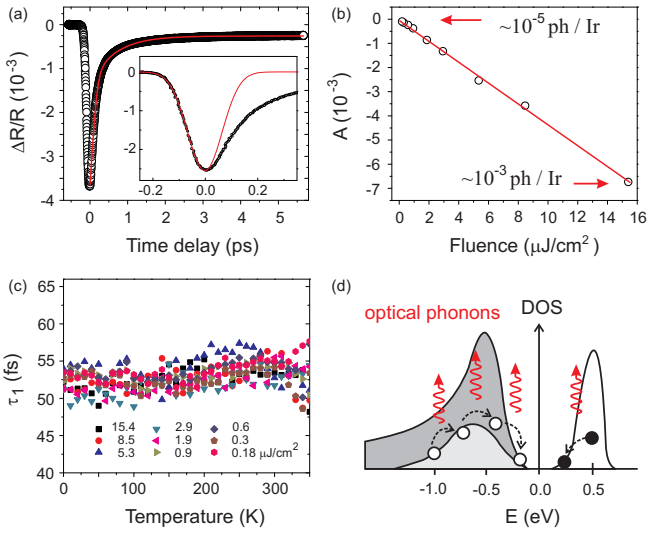

FIG. 3. (a) A typical un-normalized time-resolved reflectivity transient (ΔR/R) of Sr_2IrO_4 overlaid with a bi-exponential fit described in the text (red curve). Inset shows the Gaussian instrument time resolution (red curve) superimposed on 300 K data where decay dynamics are dominated by the fast (τ_1) component [Fig. 4(b)]. This shows that the fast initial decay is not resolution limited. (b) The fitted amplitude (A) of the fast exponential decay component measured over a range of pump fluences corresponding to $\sim 10^{-5}$ to $\sim 10^{-3}$ pump photons per iridium atom. The red line is a linear fit. (c) Temperature dependence of the fitted decay time (τ_1) of the fast exponential decay component measured over a range of pump fluences. (d) Schematic showing that the initial fast decay process is governed by energy relaxation of photo-excited electrons and holes towards the band edges via optical phonon emission. The errors in the fit parameters are less than size of the symbols.

that the Debye temperature of Sr_2IrO_4[16] far exceeds our measurement temperatures, we conclude that the initial fast recovery of ΔR/R is due to the cooling of photo-excited carriers via generation of hot optical phonons [Fig. 3(d)].

B. Slow decay component

The initial fast recovery of ΔR/R is followed by a second slower decay component, whose amplitude (B) exhibits an upturn upon cooling the starting equilibrium temperature of the system through T_N and then ceases to grow further below a temperature $T_G = 175$ K [Fig. 4(a)]. The amplitude of the fast component (A) shows comparatively little temperature dependence [Fig. 4(a)], therefore the temperature dependence of their relative amplitude (B/A) is dominated by the features observed in B [Figs. 4(b) and (c)]. This indicates that at temperatures far above T_N the electronic energy relaxation occurs predominantly through the lone process of optical phonon generation described in Figure 3 and that a separate re-

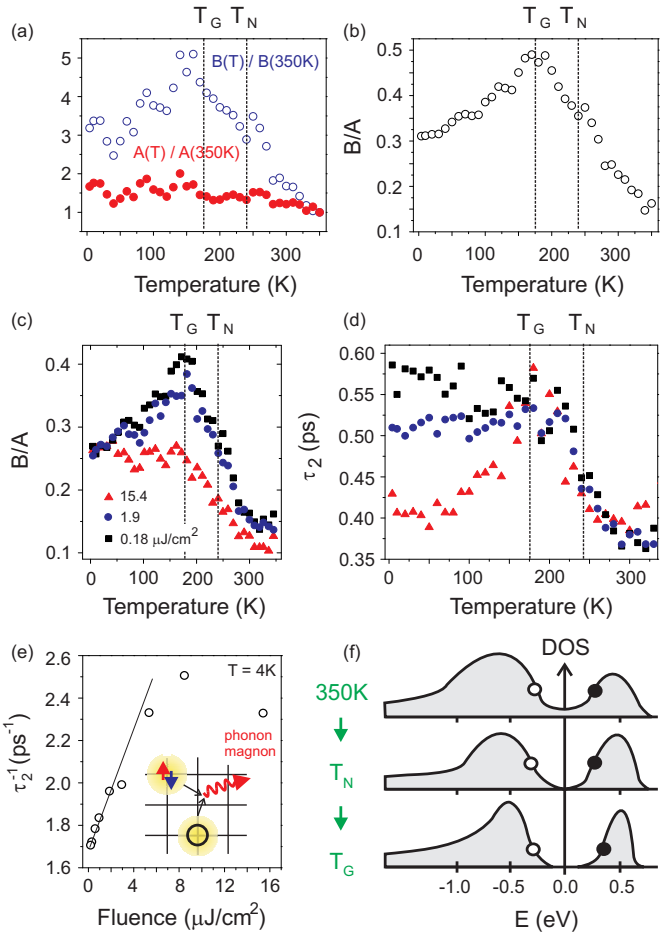

FIG. 4. (a) Temperature dependence of the fit parameters A and B, normalized to their values at $T = 350$K, taken in the low pump fluence regime. (b) Temperature dependence of B/A derived from data shown in (a) and (b). (c) Temperature dependence of the amplitude ratio and (d) the decay time of the slower component (τ_2) measured using three different fluences 15.4 μJ/cm^2, 1.9 μJ/cm^2 and 0.18 μJ/cm^2. (e) Fluence dependence of the slower decay rate measured at 4 K. Straight line is a guide to the eye showing a linear dependence at low fluences. The errors in the fit parameters are less than size of the symbols. A schematic of the bimolecular relaxation process involving the annihilation of photo-excited empty and doubly-occupied sites via emission of optical phonons or magnons is shown in the inset, which emphasizes the Mott-Hubbard character of the system. (f) Schematic showing the temperature evolution of the low energy electronic density of states (DOS) in Sr_2IrO_4 based on our data.

laxation mechanism grows near T_N before saturating below T_G. The decay time τ_2 shows a similar upturn upon cooling through T_N from around 0.36 ps at 350 K to 0.55 ps at T_G and then exhibits a marked change in temperature dependence below T_G [Fig. 4(d)]. A sharp rise in relaxation time at T_N typically signifies the development of an energy gap[20,21], where a depletion of states around E_F greatly reduces the efficiency of photo-carrier relaxation from above to below E_F.

The hallmark of a fully formed energy gap is that photo-excited occupied states above E_F and empty states below E_F can only combine in a pairwise fashion. Therefore, unlike in a metal, the recombination rate should be proportional to the density of photo-excited electron-hole pairs[26]. We find that a clear fluence dependence of τ_2 develops only below T_G [Fig. 4(d)] and that the low temperature relaxation rate τ_2^{-1} indeed increases linearly with fluence below 5 μJ/cm^2 [Fig. 4(e)]. This shows that below T_G, τ_2 represents the timescale for recombination of photo-excited electron-hole pairs across the insulating gap, which in the Mott-Hubbard limit corresponds to the recombination of singly- and doubly-occupied sites [inset Fig. 4(e)]. This ultrafast sub-ps recombination time in Sr_2IrO_4 is comparable to that observed in the 2D antiferromagnetic cuprate Mott insulators[27], which has been attributed to additional recombination channels involving hot magnon generation. Altogether these observations allow us to conclude that at temperatures far above T_N the system behaves like a metal. Near T_N the density of states around E_F is continually depleted upon cooling, which is consistent with optical conductivity measurements[19], and the insulating gap is fully developed below T_G.

To rule out the possibility that the observed temperature dependent features are artifacts of cross-correlation between our five fitting parameters, we note that based on figures 3(c) and 4(a) the parameters A and τ_1 exhibit no pronounced features at the temperatures of interest T_N and T_G. Moreover, we show in the following section that the feature at T_N observed in the temperature dependence of C is completely independent of the fitted parameters associated with the two exponential decays. Therefore the only parameters that show features at T_N and T_G and may be inter-dependent are B and τ_2. However the fitting errors associated with B and τ_2 are very small (Fig. 2), which is further support that their temperature dependence is real and robust.

The occurrence of the metal-to-insulator transition at T_N in Sr_2IrO_4 (Fig. 4) distinguishes it from archetypal Mott insulators such as MnO where the insulating gap persists even in the absence of long-range magnetic order[28]. The continuous nature of the MIT and its development over a broad ($0.7 \lesssim T/T_N \lesssim 1.4$) temperature window further precludes a Mott-Hubbard description, which predicts sharp first-order MIT's like in V_2O_3[28]. Although our measurements do not rule out gaps beginning to form in microscopically segregated regions above a bulk MIT temperature (T_{MIT}), such as the case in doped V_2O_3[29], the fact that such gap opening takes place exactly across T_N in Sr_2IrO_4 defies a strict Mott-Hubbard description. We rule out the possibility of a disorder broadened T_{MIT} in our samples based on their sharp magnetic susceptibility curves[3,17]. Although these results point towards a second-order Slater-type MIT, Sr_2IrO_4 does not conform to a weakly correlated ($U \ll W$) spin-density wave description, which are driven

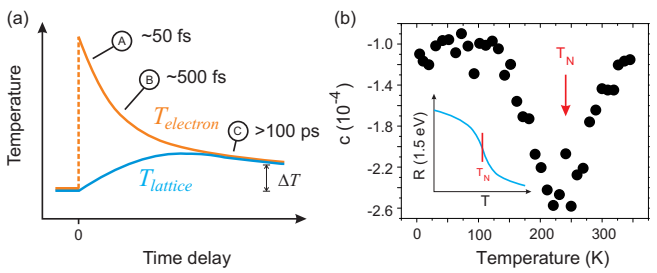

FIG. 5. (a) Diagram illustrating the temporal equilibration between the electronic and lattice sub-systems following a pump pulse. The slowest process (C) is the cooling of the equilibrated system via diffusion of hot carriers or hot phonons away from the measured sample spot. (b) Temperature dependence of the offset (C) measured using a fluence of 15.4 μJ/cm^2. A clear minimum in C is observed at T_N corresponding to a rapid rise in reflectivity at 1.5 eV at T_N (see inset schematic). The errors in the fit parameters are less than size of the symbols.

purely by Fermi surface nesting and are typically only partially gapped below T_N. Unlike a conventional spin-density wave system, magnetic ordering in Sr_2IrO_4 does not change the size of the unit cell[11] and local moment fluctuations exist well above T_N according to both magnetic susceptibility[3,17] and magnetic diffuse x-ray scattering measurements[30]. While these magnetic signatures provide evidence for correlation physics at play, a direct electronic distinction between a correlation driven MIT and a Fermi surface nesting driven MIT is whether or not, respectively, spectral weight is transferred from low (near E_F) energies to high (of order U) energies upon traversing the MIT[31].

C. Offset component

To determine whether the in-gap spectral weight lost at T_N is being transferred to upper and lower Hubbard bands, we investigate the temperature dependence of the optical reflectivity at the energy scale of optical transitions from the occupied $J_{eff} = 1/2$ and $J_{eff} = 3/2$ bands to the unoccupied $J_{eff} = 1/2$ band [inset Fig. 1(a)] by studying the small negative offset term C in the un-normalized ΔR/R traces. The two exponential relaxation processes have been identified as intra-band cooling and recombination processes that both lead to a transfer of energy from the electronic to lattice sub-systems, which brings them into thermal equilibrium within the first few ps [Fig. 5(a)]. Subsequent cooling of this heated sample spot back to the initial temperature takes place through the diffusion of hot carriers or hot phonons away from the laser illuminated area, which is estimated to well exceed 100 ps based on thermal conductivity and heat capacity data for Sr_2IrO_4[16]. To estimate the time required for heat to escape the laser excited region of the Sr_2IrO_4 crystal, we calculate its thermal diffusivity $D_{th} = \frac{k}{\rho c}$ where k is the thermal conductivity, ρ is the density and c is the specific heat. We use the values measured at $T = 100$ K in[16] of $k = 2.5$ W/m.K, $\rho = 7440$ kg/m^3 and $c = 30$ J/kg.K, which yields $D_{th} = 1.1 \times 10^{-5}$ m^2/s. From this we estimate the time needed for heat to diffuse out of a 1μm^2 area to be around 1 ns. Therefore to a very good approximation the offset C is a measure of the fractional change in reflectivity at 1.5 eV due to a small temperature change ΔT [Fig. 5(a)], namely C $= \frac{R(T+\Delta T)-R(T)}{R(T)}$. We estimate that at high pump fluences ΔT is of order 1 K because C is of order 10^{-4} and the fractional decrease in optical conductivity at 1.5 eV is estimated to be 2% from 10 K to 500 K[19]. The ability to resolve such small temperature induced changes in reflectivity is an advantage our non-equilibrium technique over conventional equilibrium optical spectroscopy. Figure 5(b) shows that the temperature dependence of C exhibits a broad negative peak with an extremum exactly at T_N, which indicates that a small temperature rise causes the largest decrease of the 1.5 eV reflectivity exactly at T_N. From this we can infer a broad temperature window ($0.6 \lesssim T/T_N \lesssim 1.4$) within which R(1.5 eV) starts to rise sharply with cooling, with the greatest slope occuring at T_N [inset Fig. 5(b)]. The fact that this temperature window largely coincides with that over which τ_2 increases most drastically [Fig. 4(d)] is consistent with a Mott-Hubbard mechanism where spectral weight is transferred from low in-gap energies (~0.1 eV[12]) to energies (1.5 eV) far exceeding it.

To demonstrate that this behavior is independent of our fitting procedure, we show that the temperature dependence of the long time offset in $\Delta R/R$, the asymptotic value of the un-normalized reflectivity variation after the first two fast decay processes, can be obtained even without fitting. Figure 6(a) shows that between $T = 4$K and 130K, this asymptotic value does not show a measurable systematic variation with temperature. Upon heating from 140K to 240K [Fig. 6(b)], the offset clearly decreases with heating and upon heating further from 250K to 350K [Fig. 6(c)], the offset exhibits a clear increase with heating. By plotting the value of $\Delta R/R$ at 5 ps as a function of temperature [Fig. 6(d)], we can already visualize the temperature dependence of the offset, which is very similar to that obtained through fitting [Fig. 5(b)]. This proves that the peak observed at T_N in the offset C is independent of how we fit the initial fast dynamics.

We note that variations in reflectivity can also be caused by a narrowing or shift of Lorentz oscillators representing direct optical transitions at 1.5 eV that do not involve spectral weight redistribution, and that our measurements do not distinguish between density of states changes in the occupied $J_{eff} = 3/2$ and $J_{eff} = 1/2$ initial states versus the unoccupied $J_{eff} = 1/2$ final state. However there is no current explanation for how such changes can be induced via magnetic ordering in the $J_{eff} = 1/2$ band. Regardless, the observed temperature dependence of the quasi-equilibrium reflectivity at 1.5 eV is unusual because the relaxation rate behavior

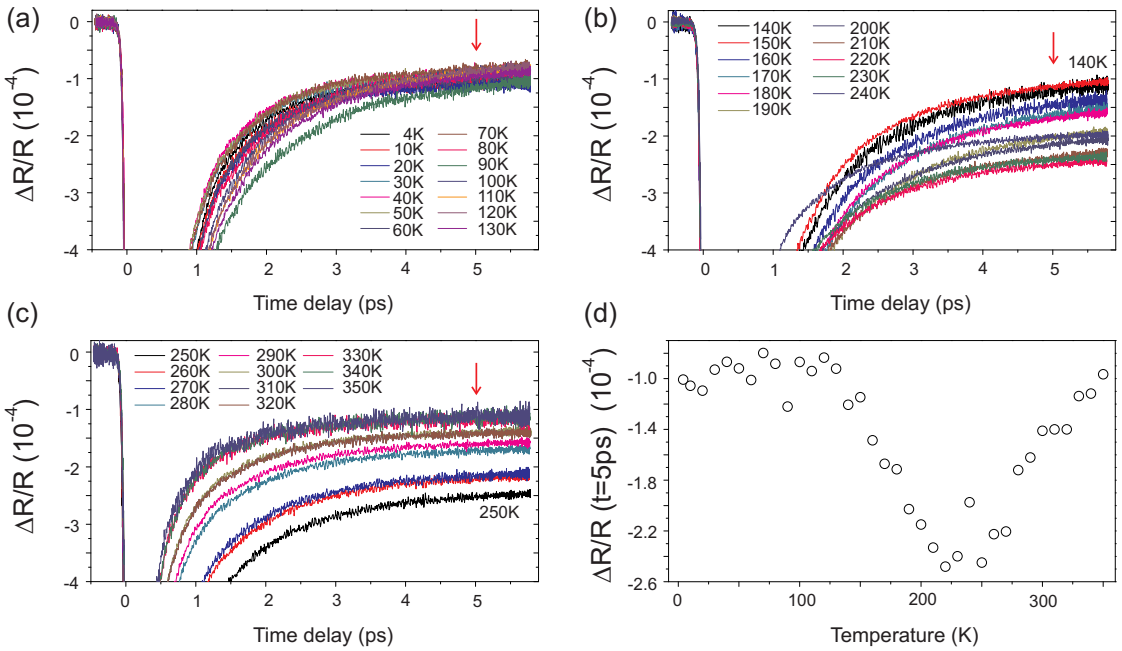

FIG. 6. Temperature dependence of un-normalized $\Delta R/R$ traces that are plotted over a range to emphasize the long time offset. Data are plotted from (a) T = 4K to 130K, (b) 140K to 240K and (c) 250K to 350K in increments of 10K. (d) The value of $\Delta R/R$ at a time delay of 5ps [red arrows in panels (a) to (c)] plotted as a function of temperature.

suggests a Slater-type behavior [Fig. 4], which should be dominated by low energy physics near the Fermi level and have little effect on the high energy reflectivity.

IV. CONCLUSIONS

Our results taken altogether suggest that unlike La_2CuO_4, which remains a Mott insulator far above its magnetic ordering temperature, Sr_2IrO_4 undergoes a metal-to-insulator transition across T_N. This suggests that Sr_2IrO_4 is more accurately described as an intermediate coupling ($U \approx W$) insulator that exhibits both Mott-Hubbard and Slater-type characteristics. Our observation that this metal-to-insulator transition takes place over a wide temperature window compared to T_N naturally explains the lack of sharp anomalies at T_N in transport, thermodynamic and optical conductivity data. We argue that these may be signatures of a rare example of a temperature controlled continuous metal-to-insulator transition in a quasi-two dimensional system hitherto unobserved in any d-electron material[28], and may be also applicable to the wider class of J_{eff}=1/2 Mott insulating perovskite, honeycomb, hyperkagome and pyrochlore iridates. Moreover, transport data on 5d Os oxides suggestive of continuous metal-to-insulators transitions[32] show that the confluence of strong spin-orbit coupling and on-site Coulomb interactions is a general playground for unconventional metal-to-insulator transitions.

Acknowledgements.

We thank F. Wang, T. Senthil, A. Vishwanath, S. Kehrein, K. Michaeli, R. Flint, S. Drapp cho and Y. Wang for useful discussions.

N. G. acknowledges support by Army Research Office grant number W911NF-11-1-0331. C. G.. acknowledges support through NSF grants DMR-0856234 and EPS-0814194.

[1] B. J. Kim *et al.*, Phys. Rev. Lett. **101**, 076402 (2008).
[2] H. Okabe *et al.*, Phys. Rev. B **84**, 115127 (2011).
[3] G. Cao, J. Bolivar, S. McCall, J. E. Crow and R. P. Guertin, Phys. Rev. B **57**, R11039 (1998).
[4] D. Pesin and L. Balents, Nature Phys. **6**, 376-381 (2010).
[5] B.-J. Yang and Y. B. Kim, Phys. Rev. B **82**, 085111 (2010).
[6] X. Wan, A. M. Turner, A. Vishwanath and S. Y. Savrasov, Phys. Rev. B **83**, 205101 (2011).
[7] M. J. Lawler, H.-Y. Kee, Y. B. Kim and A. Vishwanath, Phys. Rev. Lett. **100**, 227201 (2008).
[8] Y.-Z. You, I. Kimchi and A. Vishwanath, <http://arxiv.org/abs/cond-mat/1109.4155> (2011).
[9] F. Wang and T. Senthil, Phys. Rev. Lett. **106**, 136402 (2011).
[10] C. Martins, M. Aichhorn, L. Vaugier and S. Biermann, Phys. Rev. Lett. **107**, 266404 (2011).
[11] B. J. Kim *et al.*, Science **323**, 1329-1332 (2009).
[12] H. Watanabe, T. Shirakawa and S. Yunoki, Phys. Rev. Lett. **105**, 216410 (2010); H. Jin, H. Jeong, T. Ozaki and J. Yu, Phys. Rev. B **80**, 075112 (2009).
[13] R. Arita, J. Kunes, A. V. Kozhevnikov, A. G. Eguiluz and M. Imada, Phys. Rev. Lett. **108**, 086403 (2012).
[14] G. Jackeli and G. Khaliullin, Phys. Rev. Lett. **102**, 017205 (2009).
[15] N. F. Mott, Metal-Insulator Transitions (Taylor & Francis, London, 1990); F. Gebhard, The Mott Metal-Insulator Transition (Springer, Berlin, 1997).
[16] N. S. Kini, A. M. Strydom, H. S. Jeevan, C. Geibel and S. Ramakrishnan, J. Phys.: Condens. Matter **18**, 8205-8216 (2006).
[17] S. Chikara *et al.*, Phys. Rev. B **80**, 140407(R) (2009).
[18] M. Ge *et al.*, Phys. Rev. B **84**, 100402(R) (2011).
[19] S. J. Moon *et al.*, Phys. Rev. B **80**, 195110 (2009).
[20] N. Gedik *et al.*, Phys. Rev. B **70**, 014504 (2004).
[21] E. E. M. Chia *et al.*, Phys. Rev. B **74**, 140409(R) (2006).
[22] J. Hohlfeld, J.G. Mller, S.-S.Wellershoff, E. Matthias, Appl. Phys. B **64**, 387390 (1997).
[23] I. Simon, J. Opt. Soc. Am. **41**, 336 (1951).
[24] H. J. Bowlden and J. K. Wilmshurst, J. Opt. Soc. Am. **53**, 1073 (1963).
[25] J. S. Lee, Y. Krockenberger, K. S. Takahashi, M. Kawasaki and Y. Tokura, Phys. Rev. B **85**, 035101 (2012).
[26] A. Rothwarf and B. N. Taylor, Phys. Rev. Lett. **19**, 27 (1967).
[27] H. Okamoto *et al.*, Phys. Rev. B **83**, 125102 (2011).
[28] M. Imada, A. Fujimori and Y. Tokura, Rev. Mod. Phys. **70**, 10391263 (1998).
[29] S. Lupi *et al.*, Nature Comm. **1**, 105 (2010).
[30] S. Fujiyama *et al.*, <http://arxiv.org/abs/1203.1983> (2012).
[31] G. Kotliar and D. Vollhardt, Phys. Today **57**, March, 53 (2004).
[32] D. Mandrus *et al.*, Phys. Rev. B **63**, 195104 (2001); Y. G. Shi *et al.*, Phys. Rev. B **80**, 161104(R) (2009).